BIOCHEMISTRY
including biophysical chemistry & molecular biology

Article

pubs.acs.org/biochemistry

Terms of Use

Distance Mapping in Proteins Using Fluorescence Spectroscopy: Tyrosine, like Tryptophan, Quenches Bimane Fluorescence in a Distance-Dependent Manner

Amber M. Jones Brunette and David L. Farrens*

Department of Biochemistry and Molecular Biology, Oregon Health and Science University, Portland, Oregon 97239-3098, United States

Supporting Information

ABSTRACT: Tryptophan-induced quenching of fluorophores (TrIQ) uses intramolecular fluorescence quenching to assess distances in proteins too small (<15 Å) to be easily probed by traditional Forster resonance energy transfer methods. A powerful aspect of TrIQ is its ability to obtain an ultrafast snapshot of a protein conformation, by identifying "static quenching" (contact between the Trp and probe at the moment of light excitation). Here we report new advances in this site-directed fluorescence labeling (SDFL) approach, gleaned from recent studies of T4 lysozyme (T4L). First, we show that like TrIQ, tyrosine-induced quenching (TyrIQ) occurs for the fluorophore bimane in a distance-dependent fashion, although with some key differences. The Tyr "sphere of quenching" for bimane (≤10 Å) is smaller than for Trp (≤15 Å, Cα−Cα distance), and the size difference between the quenching residue (Tyr) and control (Phe) differs by only a hydroxyl group. Second, we show how TrIQ and TyrIQ can be used together to assess the magnitude and energetics of a protein movement. In these studies, we placed a bimane (probe) and Trp or Tyr (quencher) on opposite ends of a "hinge" in T4L and conducted TrIQ and TyrIQ measurements. Our results are consistent with an ∼5 Å change in Cα−Cα distances between these sites upon substrate binding, in agreement with the crystal structures. Subsequent Arrhenius analysis suggests the activation energy barrier (E_a) to this movement is relatively low (∼1.5−2.5 kcal/mol). Together, these results demonstrate that TyrIQ, used together with TrIQ, significantly expands the power of quenching-based distance mapping SDFL studies.

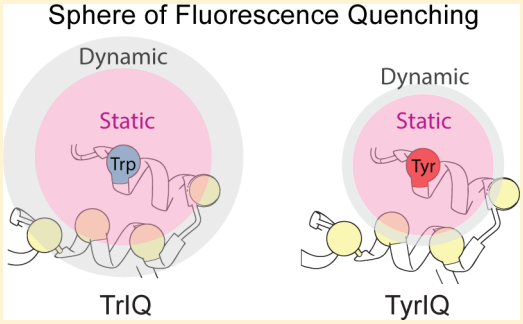

Methods for studying protein dynamics still lag behind those for determining structure, although alternative methods, like site-directed fluorescence labeling (SDFL), are showing increasing promise and are being increasingly used.[1−14] Our lab and others have been developing SDFL methods that exploit the small size and excellent spectral properties of the fluorophore bimane, with the goal of improving the resolution and ability of SDFL methods to study protein structure and dynamics. One especially powerful method we have developed, called tryptophan-induced quenching (TrIQ), can map interactions within and between proteins as well as assess protein movements in real time, by monitoring changes in the distance-dependent quenching of certain fluorophores caused by a nearby Trp residue.[15−26] TrIQ has some unique advantages that make it complementary to FRET; it operates only over relatively short distances (<15 Å) and does not require labeling a sample with two different fluorescent probes. TrIQ also does not require quantitative label incorporation, because the quencher (Trp) is always encoded in the protein (see Figure 1). Perhaps the most powerful aspect of TrIQ lies in its ability to identify and quantify "static quenching",[18−20,27] a situation in which the fluorophore/Trp pairs are so close they are already touching when the photon is absorbed (see Figure 2). Such data provide a near-instant snapshot of a given protein conformation.

Here we set out to expand this SDFL approach by testing if the amino acid tyrosine (Tyr) can also be used as a quenching residue and, if so, determining how the use of Tyr as a quencher could enhance protein studies. To do this, we calibrated the distance-dependent ability of Tyr to quench the fluorophores bimane and BODIPY 507/545 while attached to T4 lysozyme (T4L). This work was spurred by previous observations by Kosower (and subsequently our lab) that free tyrosine methyl ester can quench bimane fluorescence in solution[18,21,28] as well as our growing realization that the increasing use of bimane derivatives in SDFL studies[15−26,29−32] requires that the effect of Tyr on bimane be fully defined to allow proper interpretation of SDFL data.

As discussed below, our results show Tyr-induced quenching (TyrIQ) is intriguingly similar to as well as clearly different from Trp-induced quenching (TrIQ). We also show how these differences could be exploited to study the magnitude and energetics underlying a "hinge bending" movement in T4L that

Received: April 24, 2014
Revised: August 18, 2014
Published: August 21, 2014

 © 2014 American Chemical Society dx.doi.org/10.1021/bi500493r | Biochemistry 2014, 53, 6290−6301

occurs upon substrate binding.[33,34] Together, our data highlight unique aspects of using Tyr as a quencher and demonstrate how a combined use of TrIQ and TyrIQ in parallel significantly enhances the resolution and ability of these SDFL methods to study protein dynamics and energetics.

■ MATERIALS AND METHODS

Materials. Chemicals and buffer components were purchased from Fischer, except monobromobimane, which was purchased from Molecular Probes.

Buffers. Buffer A consisted of 50 mM MOPS, 50 mM Tris, and 1 mM EDTA (pH 7.6). Cell-pellet wash buffer consisted of 50 mM Tris-PO_4 (pH 7.2) and 50 mM sodium acetate. Lysis buffer consisted of 50 mM Tris-PO_4 (pH 7.2), 50 mM sodium acetate, 5 mM β-mercaptoethanol, 0.1 mM PMSF, and a 1× Complete Protease Inhibitor tablet. Binding/wash buffer consisted of 100 mM sodium phosphate (pH 7.2). Elution buffer consisted of 100 mM sodium phosphate and 100 mM sodium fluoride (pH 7.2). Regeneration buffer consisted of 100 mM phosphoric acid. Storage buffer consisted of 100 mM sodium phosphate (pH 7.2) and 0.02% sodium azide.

Construction, Expression, and Purification of T4 Lysozyme Mutants. T4 lysozyme was cloned into the pG58 vector,[35] and overlap-extension polymerase chain reaction was used to introduce point mutations into the protein. All mutant sequences were confirmed by DNA sequencing. Hereafter, mutants are named as follows: the native amino acid residue, the residue number, and the new residue. For example, a mutant called N116F has a phenylalanine residue replacing the asparagine residue at position 116.

Mutant T4 lysozyme was expressed in BL21(DE3) cells, using fresh transformants. BL21(DE3) cultures were grown to an OD_{595} of 0.9 at 18 °C while being shaken. Expression was induced by IPTG at a final concentration of 1 mM, and the culture was incubated at 37 °C for 2 h while being shaken, harvested by centrifugation, washed with cell-pellet wash buffer, and repelleted to remove as much chloride from the cell pellet as possible. Pellets were then stored at −20 °C for up to 2 weeks, until they were used.

Purification and Fluorescent Labeling of Proteins. Typically, the cell pellets for six different mutants were prepared simultaneously. Cell pellets were resuspended in lysis buffer and lysed using a Fisher French pressure cell. For the T4L T26E active site mutants, wild-type T4L lacking the Profinity tag (from Sigma-Aldrich) was added to the bacterial homogenate to help hydrolyze the peptidoglycan, because the active site mutant T4L covalently binds their substrate and does not turn over. Major cell debris was removed by centrifugation at 14K rpm for 45 min in a Beckman JA20 rotor. The supernatant was decanted and passed through a 0.8 μm filter to remove insoluble lysate and then loaded on an equilibrated Profinity eXact resin (which will bind only the tagged lysozyme mutants) and washed with at least 15 column volumes of binding/wash buffer, in a gravity flow apparatus.

Fluorescent labeling of the T4L samples was conducted while the proteins were bound to the purification column. First, the resin-bound T4L was incubated with an estimated 5-fold molar excess of monobromobimane label in binding/wash buffer or a 5-fold excess of BODIPY 507/545 iodoacetamide in binding/wash buffer containing 10% dimethyl sulfoxide (DMSO) for 2 h at room temperature with nutation. Subsequently, the labeling buffer was drained and the column washed with 15 column volumes of binding/wash buffer for bimane-labeled samples; when labeling was conducted with BODIPY 507/545, the first 5 column volumes of wash also contained 10% DMSO to remove unreacted label. Fluorescently labeled T4L was eluted by incubating the column in elution buffer overnight at room temperature with nutation. The eluate was concentrated and buffer exchanged with buffer A with an Amicon Ultra centrifugal filter (0.5 mL, 10 kDa), for a final exchange dilution of >1/3000, which also removed free fluorescent label (to <1%) and allowed for buffer exchange from elution buffer to buffer A.

Hydrolysis of Peptidoglycan Bound to the Active Site of the T4L T26E Mutants. The peptidoglycan bound to the active site of the T4L T26E mutants was acid-hydrolyzed essentially as described by Kuroki et al. when they first described this mutation.[33] Samples were buffer exchanged with an Amicon Ultra centrifugal filter (0.5 mL, 10 kDa) to a buffer containing 50 mM NaH_2PO_4 and 50 mM sodium acetate (pH 3) and incubated for 1 h at 37 °C. The samples were then returned to buffer A, also using Amicon Ultra centrifugal filters.

Fluorescence Intensity Measurements. To allow direct comparison of the data, sample concentrations were adjusted by dilution so they had matching fluorophore maximal absorbances for bimane (typically Abs = 0.05, and absorbance maxima ranged from 386 to 397 nm depending on bimane location) and for BODIPY 507/545 at 507 nm. Fluorescence intensity measurements were taken using a PTI Quanta Master fluorometer (PTI). Bimane excitation was at 380 nm (1 nm slits), while emission was scanned from 400 to 650 nm (8 nm slits using a 0.2 s integration time per 1 nm step size). The total bimane fluorescence was obtained by integrating the fluorescence from 400 to 650 nm for each bimane-labeled sample. BODIPY 507/545 excitation was at 480 nm (1 nm slits), while emission was scanned from 500 to 700 nm (3 nm slits using a 0.2 s integration time per 1 nm step size). The total BODIPY 507/545 fluorescence was obtained by integrating the fluorescence from 500 to 700 nm for each BODIPY 507/545-labeled sample.

Quantum Yield Measurements. The quantum yield of bimane was calculated by comparing its absorbance and fluorescence intensity at 360 nm to those of quinine sulfate, a common fluorescent standard that has a quantum yield of 0.54 in 1 N H_2SO_4, using the following equation.

$$\phi_{\text{sample}} = \phi_{\text{std}} \times \frac{F_{\text{sample}}}{F_{\text{std}}} \times \frac{\text{Abs}_{\text{std}}}{\text{Abs}_{\text{sample}}}$$

Quantum yields were calculated for T4L N116F/N132B, N116F/N132B, N116Y/N132B, and N116W/N132B to test the merits of using Phe as the nonquenching control residue instead of the native residue, as previously used.

Fluorescence Lifetime Measurements. Fluorescence lifetime measurements were taken using a PicoQuant FluoTime 200 time-correlated single-photon counting instrument (PicoQuant, Berlin, Germany), outfitted with a Hamamatsu microchannel plate detector, using polarizers at magic angle and 8 nm emission slits. Excitation was achieved using a pulsed diode laser of 405 nm, which yielded an instrument response function (IRF) of 64−128 ps [full width at half-maximum (fwhm)] measured using a Ludox solution. Emission from the samples was collected using a stack of two 470 nm long-pass filters on the detector side of the sample holder using the same slits and the same polarization. The fluorescence decay curves were fit with PicoQuant software using an exponential decay model [$I(t) = \sum_{i-1}^{n} A_i e^{-t/\tau_i}$, where A_i is the amplitude of the ith

component in counts, in the first range fitting channel and τ_i is the lifetime of the ith component]. The quality of each fit was assessed by considering the χ^2 value, the residuals, and the autocorrelation function. In some cases, fits with higher χ^2 values were chosen because the residuals and autocorrelation functions were more randomly distributed and had lower values. The amplitude weighted average lifetime ($\langle\tau\rangle$) resulting from the best fit were used in calculations as discussed below.

The lifetime decay data were also fit with a Lorentzian distribution model $\{I(t) = \int_{-\infty}^{t} \mathrm{IRF}(t') \int_{-\infty}^{\infty} \rho(\tau) e^{-t-t'/\tau}\, d\tau\, dt'$ $\rho(\tau) = \sum_{i=1}^{n} (A_i/\pi)[\Delta_{(\mathrm{fwhm}\ i/2)}/(\tau - \tau_i)^2 + \Delta_{(\mathrm{fwhm}\ i/2)}{}^2]$, where A_i is the amplitude of the ith distribution component, in counts, in the first range fitting model, τ_i is the center lifetime of the ith distributed component, and $\Delta_{\mathrm{fwhm}\ i}$ is the distribution width (full width at half-maximum) of the ith distributed component}. The results and discussion for the distribution fitting can be found in the Supporting Information.

Calculation of the Fraction of the Fluorophore in a Static Complex with a Quencher. The fluorescence contribution of each quencher−fluorophore pair was calculated as described previously.[18−20] Briefly, using this analysis, the relative fraction of quencher and fluorophore in an open, nonstatic conformation, called gamma (γ), is calculated with the equation $\gamma = F/F_O \times \tau_O/\tau$, where F is the fluorescence intensity and τ is the lifetime (the subscript O refers to the Phe-containing unquenched measurement). It is also possible to further separate γ into the contribution by dynamic quenching [$\gamma_{DQ} = (1 - \tau/\tau_O)\gamma$] and the contribution from unquenched fluorescence ($\gamma_O = \tau/\tau_O \times \gamma$). The relative fraction of quencher−fluorophore pairs in a static (nonfluorescent) complex at the moments of light excitation is then simply determined as $1 - \gamma$.

Analysis of the pH Dependence of the TrIQ and TyrIQ Effects. The purified and labeled T4L mutants N116F/N132B, N116Y/N132B, and N116W/N132B were buffer exchanged into a 50 mM $NaPO_4$, 50 mM sodium acetate buffer at pH 3, 7.5, and 10. The fluorescence intensity and lifetime decay were measured as described above for each of the mutants at each of the three pH conditions at 20 °C. The fraction of the fluorophore in a static complex with the quencher was calculated for each pH condition as described above.

Arrhenius Analysis of Hinge Bending and Temperature Dependence of the TrIQ and TyrIQ Effects. The fluorescence intensity and lifetime decay were measured as described above but with the F4/K60B, F4Y/K60B, and F4W/K60B mutants at 10, 15, 20, 25, and 30 °C to evaluate the temperature dependence of the TrIQ effect and were used for Arrhenius analysis.

The same measurements were also taken on mutants containing the T26E active site mutation, which traps the substrate by making a noncatalytically relevant covalent bond between T4L and the peptidoglycan. For these studies, the bound substrate was hydrolyzed prior to the measurements described above, lifetime decays were fit with an exponential decay, and the amplitude-weighted average lifetimes ($\langle\tau\rangle$) from the best fits were used to calculate the dynamic quenching rate using the equation $k_q = 1/\tau - 1/\tau_O$. The natural log of k_q was plotted on the y-axis against the reciprocal of the sample temperature in kelvin on the x-axis. The slope of the resulting line is taken to be the activation energy divided by the gas constant ($-E_a/R$) from the Arrhenius equation.

The average lifetime ($\langle\tau\rangle$) was used for the sake of simplicity in the dynamic quenching rate calculations because multiple apparent lifetimes are detected in the TrIQ and TyrIQ data, especially ultrashort lifetimes in samples with extensive quenching (see Table 1 of the Supporting Information). We attribute the latter very fast quenching events to quenchers that are next to, but not touching, the fluorophore at the moment of light excitation. Such phenomena are not due to multiple distinct probe environments but rather occur because the limited diffusional volume space for the fluorophore and quencher (due to their being covalently attached to the protein) results in a very high apparent quencher concentration (see the discussion in Chapter 9.6 of ref 36).

RESULTS

Our goal was to determine if the amino acid Tyr, like Trp, could be used as an internal quenching molecule in SDFL studies for mapping proximity in proteins. To do this, we compared the extent of Trp-induced quenching (TrIQ) and Tyr-induced quenching (TyrIQ) on the emission from the fluorophores bimane and BODIPY 507/545 (Figure 1), while

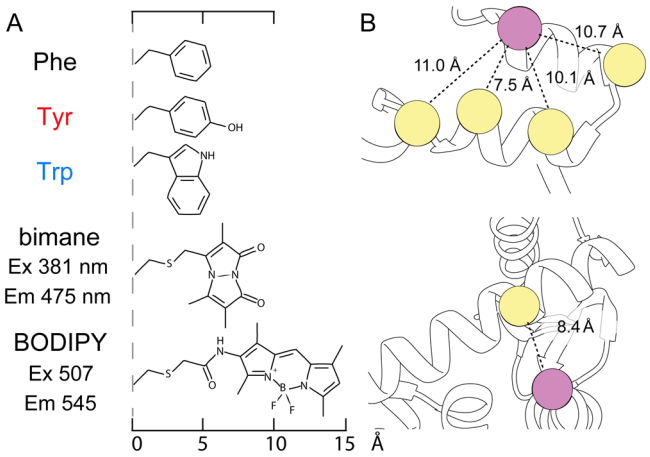

Figure 1. Model showing the fluorophores, quenching residues, and sites of attachment on T4 lysozyme used in this study. (A) Structures and abbreviations for the quenching and nonquenching residues (Trp, Tyr, and Phe) and fluorophores (bimane and BODIPY 507/545). The spectral qualities of the fluorophores are listed below the name. (B) Model of T4 lysozyme (top) highlighting the location of the Cα atoms of the cysteines used for fluorophore incorporation using SDFL at sites 123, 128, 132, and 135 (yellow spheres). The location of the fifth cysteine site, at position 68, is shown below. The pink spheres indicate the Cα atoms of sites N116X (top) and F4X (bottom), where X is phenylalanine (F), tryptophan (W), or tyrosine (Y). The different Cα−Cα distances between the probe and quencher site are also indicated. The models were generated using coordinates from PDB entry 1L63 and the UCSF Chimera package.

these probes were attached to the sites on the protein T4L indicated in Figure 1B. These sites provided varying probe−quencher distances, ranging from ∼7 to 11 Å (Cα−Cα distances). The data from these studies could be analyzed to determine the relative fraction of fluorescence present in each sample (nonquenched, dynamically quenched, and statically quenched, as described in the legend of Figure 2). The results are discussed below.

Phenylalanine Is a Structurally Similar Control Residue for TyrIQ and TrIQ Studies That Shows Minimal Bimane Quenching. We tested if Phe, a residue structurally similar to Tyr and Trp, could act as a better "control" (nonquenching residue) for TyrIQ and TrIQ studies, rather

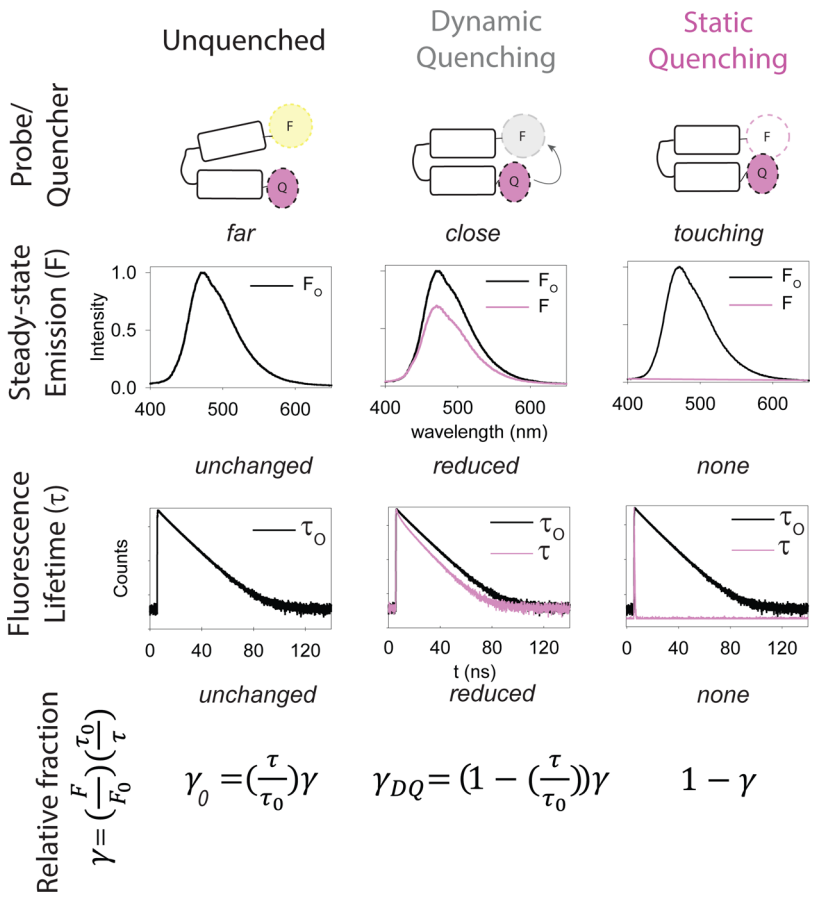

Figure 2. Models illustrating the three different quencher–fluorophore conformations that can be quantified using fluorescence measurements and how their fluorescence emission intensity and lifetime decay differ (top row). As shown, at the moment of light excitation, the quencher and fluorophore can either be far apart from each other and unable to quench (top left), close enough for the quencher to dynamically quench the fluorophore after excitation (top middle), or so close that the pair touch before light excitation, resulting in a nonfluorescent complex (top right). The effects of these different conformations on the fluorescence emission and decay are shown in the second and third rows, respectively. Note that both dynamic and static quenching results in a decrease in fluorescence intensity, yet their fluorescence decay results are drastically different. Dynamic quenching results in a faster decay in fluorescence (shorter lifetime), while fluorophores that are statically quenched have no lifetime and do not contribute to this analysis. The relative contribution of each quenching state can be elucidated from the fluorescence intensity (F_O/F) and lifetime quenching ratios ($\langle\tau_O\rangle/\langle\tau\rangle$) using the equations in the final row, as described in Materials and Methods.

Scheme 1

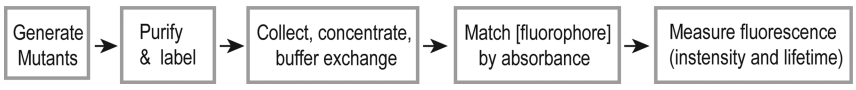

than our previous approaches that simply used whatever native residue was at the site under investigation. To do this, we studied T4L mutants containing a Phe, Tyr, Trp, or Asn (the native residue) at position 116 and a bimane fluorophore at position 132. Sites 116 and 132 show the largest amount of Trp quenching and represent the closest quencher–fluorophore pair in this study (Cα–Cα distance of 7.5 Å). The results of absorbance and fluorescence measurements on these samples are reported in Table 4 and Figure S1 of the Supporting Information. As one can see in Figure S1, the bimane absorbance maximum is red-shifted for the Phe, Tyr, and Trp samples compared to that of the sample containing the native Asn residue (~386 nm for the N116/132B sample compared to ~397 nm for the others). Such a shift in absorbance indicates the formation of a ground-state complex (contact) between the residue and bimane fluorophore, as we have noted and discussed previously.[18–20,37]

However, even with this contact, bimane quenching by Phe is minimal, as indicated in the comparison of intensity quenching ratios, calculated using N116/N132B as the unquenched control, 1.3 for the Phe-containing sample (N116F/N132B) versus ~14.0 for the Tyr-containing sample (N116Y/N132B) and ~27.0 for the Trp-containing sample (N116W/N132B). These values, along with the measured quantum yields, and relative changes in fluorescence lifetimes are reported in Table 4 of the Supporting Information. Together, these studies demonstrate Phe is an excellent control residue for TyrIQ and TrIQ studies, because of its structural similarity for both Tyr and Trp, and because it causes limited quenching even when physically in contact with bimane.

Tyrosine Can Quench the Fluorescence Intensity of Bimane in a Distance-Dependent Fashion but Does So over a Range Shorter Than That of Tryptophan. We measured the ability of both Tyr and Trp to quench bimane in

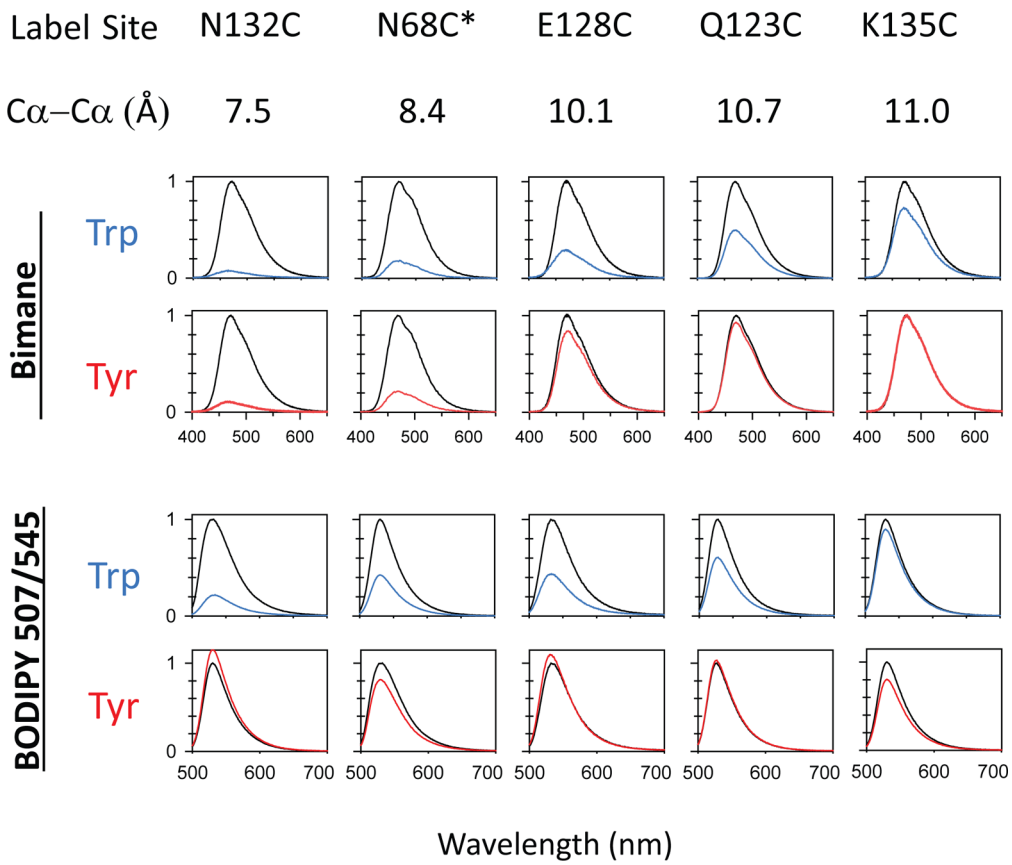

Figure 3. Fluorescence emission intensity for Phe-containing, unquenched samples (black) and samples quenched by Trp (blue) or Tyr (red) for the fluorophores bimane (top) and BODIPY 507/545 (bottom). In all cases, the Phe, Tyr, or Trp was incorporated at one of the indicated locations on T4L (site 116 or site 4 for N68C, indicated by asterisks) and a fluorophore was covalently attached to unique cysteines at multiple locations on T4L indicated in Figure 1, resulting in the indicated different Cα–Cα distances separating the quencher and probe. The data show Trp can quench bimane fluorescence, to some degree, at all distances measured, with the best quenching observed at the shortest distance and the least quenching at the longest distance. Tyr can also quench bimane at short distances but, in contrast to Trp, is unable to considerably quench bimane at separations longer than ~10 Å. Trp also quenches BODIPY 507/545 in a distance-dependent manner, whereas Tyr does not dramatically quench BODIPY 507/545 at any of the distances measured.

our studies in parallel, both for the purpose of comparison and to test the efficacy of our new streamlined purification and fluorescence labeling strategy for T4L, shown in Scheme 1. As expected, the results reconfirm our previous findings that Trp quenches bimane in a distance-dependent manner (Figure 3, top). The data show tyrosine also quenches the emission intensity of bimane but does so less efficiently and over a shorter distance range (Figure 3). For example, whereas tryptophan quenching of bimane is seen to extend to the 11.0 Å Cα–Cα distance, tyrosine exhibits essentially no quenching for Cα–Cα separations of >10 Å.

Unlike Tryptophan, Tyrosine Does Not Show Substantial Quenching of BODIPY 507/545 Fluorescence. We previously established that Trp can also efficiently quench the fluorescence of the probe BODIPY 507/545 in a distance-dependent manner.[18] Interestingly, we find here that Tyr does not show substantial quenching of BODIPY 507/545 fluorescence (Figure 3, bottom, and Figure S4 of the Supporting Information). Because these samples exhibited no dramatic fluorescence intensity quenching, they were not studied further.

The Degree of Intensity Quenching Does Not Always Match the Degree of Lifetime Quenching for Both Quenchers, Trp and Tyr. Figure 4A shows how the ratio of Trp- and Tyr-induced quenching of bimane (F_O/F) measured in Figure 3 decreases as a function of Cα–Cα distance. The quenching mechanism occurring in these samples was further investigated by measuring their fluorescence lifetimes (rates of fluorescence decay after excitation) using a PicoQuant FluoTime 200 time-correlated single-photon counting instrument with a time resolution of ~50 ps. Representative fits of the decay data can be found in Figure 2 of the Supporting Information. The amplitude-weighted average lifetime ($\langle\tau\rangle$) from the exponential fits of these decay data was used to calculate the lifetime quenching ratio, ($\langle\tau_O\rangle/\langle\tau\rangle$), as shown in Figure 4B.

For the unquenched bimane-labeled samples (Phe residue at the "quenching" position), the $\langle\tau\rangle$ values ranged from 7.9 to 13.4 ns (Table 1 of the Supporting Information), depending on the environment of the probe,[38] similar to previous reports.[18−20,37] For the Trp-containing T4L mutants, the $\langle\tau\rangle$ lifetime was observed to decrease for all of the Trp–bimane distances (7.5, 8.4, 10.1, 10.7, and 11.0 Å), with the most dramatic changes in lifetime occurring at the shorter distances. In contrast, the Tyr-containing T4L samples showed a dramatic decrease in lifetime for the 8.4 Å Tyr–bimane distances and the closest and intermediate distances (7.5 and 10.1 Å) and no decrease in the longest distances (10.7 and 11.0 Å) compared to those of the unquenched (Phe) samples. A similar pattern is

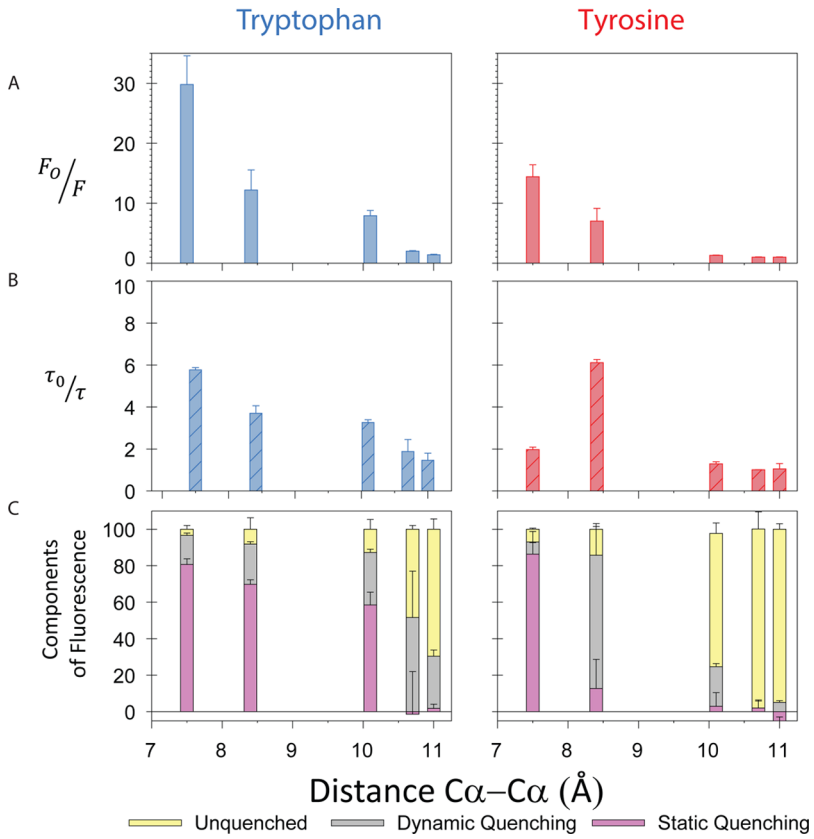

Figure 4. Comparison of the distance-dependent effect of Trp and Tyr quenching on bimane emission, fluorescence lifetime, and the calculated relative components of fluorescence quenching. (A) Ratio of the fluorescence intensity of bimane-labeled T4L samples with the probe at different Cα–Cα distances from a Phe (F_O) or either of the quenching residues, Trp or Tyr (F). The data indicate the F_O/F for Trp (blue bars, top left) is greater than for Tyr (red bars, top right) and decreases less rapidly as a function of Cα–Cα distance. The quenching ratios at each Cα–Cα distance were measured in quadruplet, except for that of the 8.4 Å sample, which was measured in triplicate. (B) Comparison of the ratio of average fluorescence lifetimes ($\langle\tau\rangle$) of bimane-labeled T4L containing a Phe at the quenching position ($\langle\tau_O\rangle$) to those of samples containing a quenching Trp (blue cross-hatched bars, middle left) or Tyr (red cross-hatched bars, middle right) ($\langle\tau\rangle$) residue at the indicated Cα–Cα distance. (C) Relative fraction of probe–quencher pairs in a static complex (and thus in direct physical contact) can be calculated using respective F_O and F, and $\langle\tau_O\rangle$ and $\langle\tau\rangle$ values. To do this, the fraction of quencher–probe pairs in a static complex is calculated as $1 - \gamma$, where γ describes the fraction of quencher–probe pairs in the "open" conformation and is given by $\gamma = F/F_O \times \tau_O/\tau$. For the open (nonstatic) quencher–probe pairs, the fraction that is not quenched is given by $\gamma_O = \tau/\tau_O \times \gamma$, and within this group, the fraction of dynamically quenched pairs is given by $\gamma_{DQ} = (1 - \tau/\tau_O)\gamma$.

observed when the decay data are fit using a lifetime distribution model, as discussed in the Supporting Information.

Differences in the Ratio of the Fluorescence Intensity and Lifetime Quenching Indicate Static Quenching Complexes Form in Some of the Trp- and Tyr-Quenched Samples. We next used the combination of intensity and lifetime quenching ratios to calculate the relative amount of static quenching, dynamic quenching, and unquenched fluorescence components (Figure 4C). This analysis shows that Trp can statically quench bimane for the 7.5, 8.4, and 10.1 Å Cα–Cα distances, whereas the quenching observed at the 10.7 and 11 Å distances is primarily dynamic in nature. These Trp quenching values for bimane show the same range of distances as our previously reported results but a higher quenching ratio. We surmise this difference in quenching ratio is due to our improved purification and labeling method (which resulted in smaller amounts of free bimane and presumably less misfolded protein).

In contrast to the Trp samples, the Tyr-containing samples showed a large amount of static quenching only at the shortest distance (7.5 Å), with much less static quenching for the 8.4 Å sample. The longer Cα–Cα distances show no static quenching for Tyr.

Assessment of the Effects of pH and Temperature on the Efficiency of Quenching for Trp and Tyr. We next tested the effect of pH and temperature on both the fluorescence intensity and lifetime decay using the N116X/N132B series of T4L mutants, where X = F, W, or Y. For both Tyr- and Trp-containing samples, both the intensity (F_O/F) and the lifetime ($\langle\tau_O\rangle/\langle\tau\rangle$) quenching ratios were measured, where an O subscript indicates data from the unquenched, Phe-containing sample.

The data show a relatively weak pH dependency for both quenchers (Figures 5 and 6 of the Supporting Information). When Trp is the quenching residue, the intensity quenching ratio slightly increases with an increase in pH (~14% per pH unit), while the lifetime quenching ratio is constant at the pH values tested. The intensity quenching ratio when Tyr is the quenching residue also follows the pattern of increasing with pH, although to a lesser extent than that of Trp (~7% per pH unit). Interestingly, the lifetime quenching ratio of Tyr does not follow a pattern, as the ratio (or decrease in the lifetime of the quenched probe relative to that of the unquenched probe at the same pH) is higher at pH 3 and 10 than at pH 7.5. When these quenching ratios are used to calculate the relative presence of static and dynamic quenching, Trp shows a constant relative

amount of each component of fluorescence (Figure 5A, top), but the relative contributions of static and dynamic quenching when Tyr is the quencher vary only slightly across the pH range tested (Figure 5A, bottom).

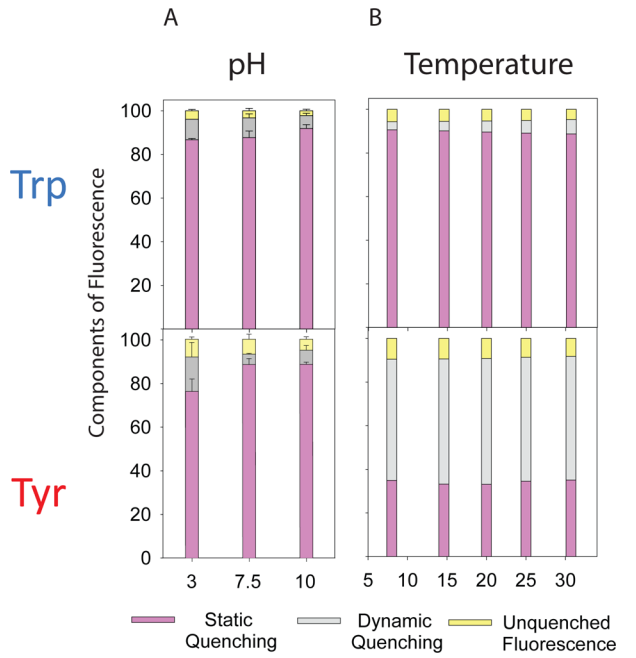

Figure 5. The pH and temperature sensitivity of TrIQ and TyrIQ components of fluorescence. TrIQ (top) and TyrIQ (bottom) components of fluorescence calculations are essentially temperature-independent (right). TrIQ is also independent of pH (bottom column), whereas TyrIQ does show some slight variation with pH (bottom row, left column). Components of bimane fluorescence were calculated for N116X/N132B samples at three different pH values (left) when they were quenched by Trp (top) and Tyr (bottom). The effects of multiple temperatures were also assessed by calculating the components of fluorescence for F4X/N68B samples across five temperatures with both Trp (top) and Tyr (bottom) as quenching residues.

We also assessed the temperature dependence of TrIQ and TyrIQ for bimane-labeled samples, using temperatures of 30, 25, 20, 15, and 10 °C. The resulting quenching ratios (F_O/F) as well as the lifetime quenching ratios ($\langle\tau_O\rangle/\langle\tau\rangle$) are shown in Figures 5 and 6 of the Supporting Information; both ratios show a slight increase with temperature for both Trp and Tyr (~1–2% per degree Celsius). The relative components of fluorescence, however, show consistent ratios of static and dynamic quenching across all of the temperatures measured for both quenchers (Figure 5B).

Both TrIQ and TyrIQ Can Detect a Hinge Bending Movement in T4L That Accompanies Substrate Binding. We next tested the ability of TrIQ to measure dynamic structural changes in T4L, specifically, a hinge bending motion that occurs in T4L upon substrate binding.[39,40] These studies placed a probe and quencher on opposite sides of this "hinge", with the probe at K60B and the quencher at site F4X, where X is a Trp, Tyr, or Phe residue, to act as the unquenched control. In the substrate-free state, the quencher and probe Cα–Cα distances are shorter (~10.5 Å apart) and move farther apart (~14.5 Å) when T4L binds the substrate (Figure 6A). Thus, one would expect more quenching in the apo state and less quenching upon substrate binding.

As expected, the results showed considerable TrIQ for the substrate-free form of the Trp-containing sample (F4W/K60B), with an intensity quenching ratio (F_O/F) of ~3.5, and the amplitude-weighted average lifetime quenching ratio ($\langle\tau_O\rangle/\langle\tau\rangle$) of ~2. This trend is repeated with Tyr as the quencher (F4Y/K60B), although the amount of quenching is much less pronounced, with an F_O/F values of ~1.5 (Figure 6B) and a $\langle\tau_O\rangle/\langle\tau\rangle$ value of ~1.2 (Table 3 of the Supporting Information), as would be expected given the decreased apparent "reach" of Tyr as a quencher.

To measure the effect of substrate binding on the structure of T4L, the same studies were conducted with samples containing an active site mutation, T26E, in the F4X/K60B background. The T26E mutation causes the peptidoglycan substrate to be covalently bound and thus traps the protein in a distinct conformation[33] with these two species separated by ~14.5 Å (Cα–Cα). For these samples, both the Trp- and Tyr-containing proteins showed a decreased level of quenching (Figure 6B). We attribute the changes in TrIQ and TyrIQ in these samples to the samples containing covalently attached peptidoglycan from the cell walls of bacteria. This was confirmed by SDS–PAGE, which shows a smear for these samples [caused by the incorporation of heterogeneous lengths of peptidoglycan polymers (see the inset in Figure 6B and Figure 7 of the Supporting Information)].

We then confirmed these differences in TrIQ and TyrIQ were due to bound peptidoglycan by incubating the T4L T26E samples for 1 h at pH 3 and 37 °C to hydrolyze the peptidoglycan–lysozyme covalent bond.[33] After these samples had been returned to the original experimental conditions of pH 7.6, the substrate-free (acid-hydrolyzed) proteins show intensity and lifetime quenching ratios similar to those of the non-active site mutant, indicating their return to the empty conformation (Figure 6B). Finally, adding back purified peptidoglycan to the acid-hydrolyzed T26E samples restored the amount of quenching to that of the static peptidoglycan-bound protein (Figure 6B).

Both TrIQ and TyrIQ Can Be Used To Assess the Energetics of a Protein Movement through Arrhenius Analysis of Dynamic Quenching Rates. We next tested the ability of both TrIQ and TyrIQ to assess the energetics underlying the hinge bending movement by measuring the fluorescence intensity and lifetime decay of the samples described above as a function of temperature. Samples with and without the T26E active site mutation were measured, at different temperatures (30, 25, 20, 15, and 10 °C), and the data were then subjected to Arrhenius analysis.

The results indicate a slight temperature-dependent change in the dynamic quenching rate, from which we calculated the activation energy for the hinge bending motion by assuming the slope of the line resulting from an Arrhenius plot of the data was equal to the activation energy divided by the gas constant, $-E_a/R$. This analysis resulted in activation energies ranging from ~1.5 to 2.5 kcal/mol (Figure 6C). The implications of these results are discussed below.

■ DISCUSSION

In this work we set out to expand and calibrate an SDFL method that is capable of mapping approximate distances within and between proteins as well as studying protein dynamics and conformational changes. Specifically, we sought to determine if Tyr, like Trp, could be used as an internal quencher in SDFL studies, as Tyr has been reported to quench

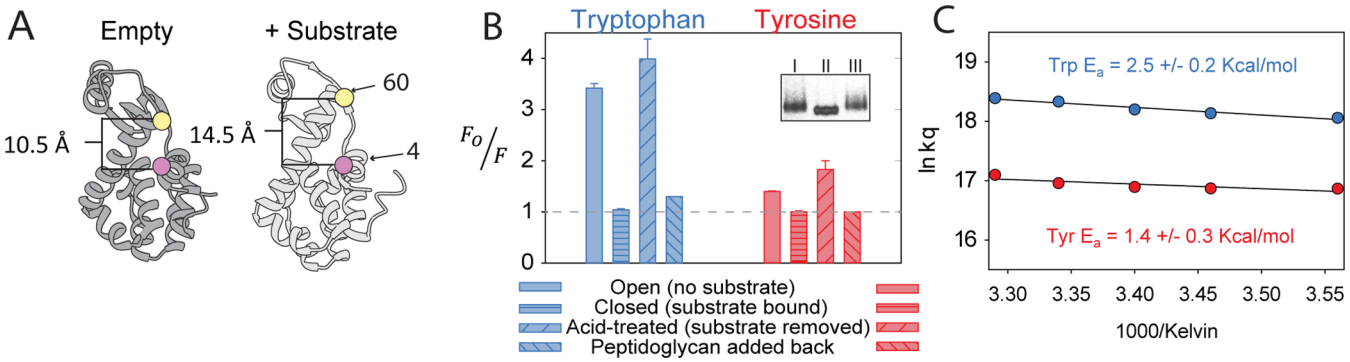

Figure 6. TrIQ and TyrIQ can be used to measure the magnitude and energetics of a hinge bending motion in T4L that occurs upon substrate binding. (A) Models of T4L both with (left) and without (right) peptidoglycan bound to the active site (PDB entries 150L and 2LZM, respectively). To monitor this change, TrIQ and TyrIQ were employed, placing the bimane probe at site 60 and the quenching residue (Trp or Tyr) or nonquenching residue (Phe) at site 4. With no substrate present, the Cα−Cα distance (angstroms) separating the quenching residue and probe is only ∼10.5 Å. When the substrate peptidoglycan binds, the Cα−Cα distance increases to ∼14.5 Å, too long for either Trp or Tyr to show substantial quenching. (B) Ratio of fluorescence emission intensity for samples containing a quenching Trp (blue line) or Tyr (red line) residue (F) compared to samples containing the nonquenching Phe residue (F_O), in the presence or absence of bound substrate. The T4L sample F4W/K60B (without substrate, empty bars) shows an $F_O/F \sim 3.5$ amount of TrIQ, which is abolished in the active site (T26E) mutant that contains peptidoglycan from the purification (horizontally hatched bars). When the bound peptidoglycan is removed by acid hydrolysis, the quenching is observed again (positive slope hatched bars), and this effect can be reversed by adding peptidoglycan to the acid-hydrolyzed samples (negative slope hatched bars). A similar but less extensive trend in TyrIQ is also observed for the T4L F4Y/K60B samples (right). The inset shows SDS−PAGE results for the respective samples showing the covalently attached peptidoglycan substrate as indicated by the slower mobility and smear in the band: T4L F4Y/T26E/K60B (I) with peptidoglycan bound, (II) when peptidoglycan is released after pH 3 incubation, and (III) after incubation with purified peptidoglycan (see Figure 7 of the Supporting Information for the full gel). (C) Arrhenius analysis of the dynamic quenching rate (k_q) from Trp- and Tyr-induced quenching of bimane in the T4L F4X/K60B mutants as a function of temperature shows similar low E_a values using either TrIQ or TyrIQ (∼1.5−2.5 kcal/mol), suggesting the energy barrier for the hinge bending movement is small. The dynamic quenching rates were calculated as described in Materials and Methods.

bimane fluorescence in the free amino acid form.[18,28] We also tested how well these internal quenching methods (TrIQ and TyrIQ) could assess the dynamics and energetics of a protein structural change, in this case, the hinge bending motion in T4L that occurs upon substrate binding.

In the process of conducting this work, we also developed a new way to purify and label the proteins (see Scheme 1), with the goal of increasing throughput and allowing future automation, as we proposed previously.[19] Briefly, this involved using the Bio-Rad Profinity eXact fusion purification method and on-column labeling of the proteins. Together with these modifications, we could substantially scale up and increase the throughput of our SDFL studies. The reduced level of sample handling and the ability to label and purify samples in parallel resulted in a 6-fold increase in sample throughput and decreased the required time from 3 days to 1. In the future, it should be possible to automate this purification and labeling approach, significantly simplifying the production of multiple samples for SDFL TrIQ and TyrIQ experiments.

Both Tyr and Trp Show Distance-Dependent Quenching of Bimane. We find that both Tyr and Trp quench bimane fluorescence in a distance-dependent manner, but there are clear differences in their abilities to do so, with Trp showing more quenching than Tyr over a longer range. Before discussing these results in detail below, we first briefly review how different types of fluorescence can be quantified in a TrIQ and TyrIQ study, followed by a discussion of the results when this analysis was applied to our samples.

There are several possible fates for a fluorophore in a TrIQ or TyrIQ study (see Figure 2). One possibility is that after absorbing light, the fluorophore is not quenched at all, and thus, the fluorescence intensity and fluorophore lifetime are unaffected. Alternatively, the fluorophore may be dynamically quenched after absorbing a photon (i.e., the quenching event occurs after absorption of a photon by the fluorophore), which results in a change in both the fluorescence intensity and lifetime. The third possibility, static quenching, is especially interesting and informative because it indicates a fluorophore and quencher are in contact with each other at the moment of light excitation.[41] Static quenching also causes a decrease in fluorescence intensity, but no similar relative change in the fluorescence lifetime τ values (because these nonfluorescent complexes emit no light, they are not detected in the lifetime measurement). Importantly, the relative amounts of each type of quenching and the relative fraction of sample in each state can be calculated as described in Figure 2 and Materials and Methods.

Subjecting our data to this analysis demonstrates that the ability of Tyr, like Trp, to exhibit static quenching of bimane depends on the distance between the quencher and bimane (Figure 4). Both quenchers show the largest relative amount of static quenching for the N116X/N132B sample, the shortest Cα−Cα distance (7.5 Å) measured here, and the Trp results reproduce our previous observations.[18−20] Static quenching due to formation of a ground-state complex between bimane and the quencher in these samples is also indicated by shifts in their absorbance spectra. As shown in Figure 1 of the Supporting Information, the absorbance λ_{max} for the bimane probe at site 132 is ∼386 nm when an Asn is at site 116 (the native residue). This absorbance λ_{max} shifts to ∼397 nm for the Tyr, Trp, and Phe samples, a strong indicator of ground-state complex formation. Importantly, these data also show that Phe causes minimal quenching of bimane, even when it is in contact with the fluorophore at the moment of light excitation (Table 4 of the Supporting Information).

Interestingly, the data show Tyr has a "maximal sphere of static quenching" that is smaller than that of Trp; that is, Tyr has an apparent reach smaller than that of Trp. In fact, Tyr exhibits no static quenching at Cα−Cα distances greater than ∼10 Å, consistent with the smaller size of Tyr compared to Trp, although the shorter apparent reach for Tyr quenching could be due to different intrinsic properties and not a difference in length. In either case, the shorter range of Tyr quenching can be used to increase resolution in mapping studies, and we show in the next section that the different ranges of quenching by Trp and Tyr can be used to resolve the magnitude of a protein conformational change, such as the hinge bending motion in T4L that occurs upon substrate binding (Figure 6).

We also explored the possibility that new information could be obtained from different analysis of the dynamic quenching component. This involved fitting the fluorescent decay data with a lifetime distribution model. Our working hypothesis was that quencher−probe pairs in very close proximity of each other, but not touching, at the moment of light excitation would exhibit ultrafast lifetimes (resulting from "pseudostatic quenching") and that separating this variable might allow further probing of the dynamic quenching component reflected in the longer lifetime component, and the results show an intriguing pattern. As shown in Figure S3 of the Supporting Information, unquenched samples were well fit by a single distribution. However, quenched species required a bimodal distribution, with an ultrafast lifetime and a longer lifetime. Intriguingly, the longer lifetime component decreases as the distance from the quencher decreases (except in the case of extreme static quenching).

We also tested the effect of pH and temperature and found that although the magnitudes of intensity quenching in TrIQ and TyrIQ are somewhat sensitive to different pH values and temperatures (Figures S5 and S6 of the Supporting Information), the effects of these parameters on the relative contribution of different components of quenching (static, dynamic, and unquenched) are not substantial (Figure 5). Only Tyr showed a slight difference in the relative contributions to static and dynamic quenching at low pH for reasons that are not presently clear but might be due to changes in the redox state of Tyr at different pH values. Despite these slight differences, we have shown here that one can still detect the presence and relative contribution of static quenching, which will allow both TrIQ and TyrIQ to be used under a range of pH and temperature conditions.

Tyr Does Not Substantially Quench BODIPY 507/545 in a Distance-Dependent Manner, whereas Trp Does. Previously, we established that Trp also quenches a number of other fluorophores besides bimane in a distance-dependent fashion, thus expanding the palette of probes that can be used in TrIQ studies.[18] Here, we reconfirmed that Trp can quench BODIPY 507/545, a red-shifted fluorophore with an excellent quantum yield. Surprisingly, we find that Tyr does not show obvious distance dependence quenching of BODIPY 507/545 (Figure 3 and Figure S4 of the Supporting Information), despite previous reports that free tyrosine methyl ester can cause some slight quenching of BODIPY 507/545 in solution.[18] In fact, analysis using a form of the Rehm−Weller equation and published redox potentials for Trp, Tyr, and BODIPY-FL[42,43] suggests that both Trp and Tyr might be able to quench some BODIPY fluorophores in a PET fashion. Unfortunately, it was not possible to conduct these calculations on the BODIPY 507/545 used here, because of a lack of published E_{red} values. Interestingly, although BODIPY 507/545 shares the same basic structure as the other BODIPY fluorophores, its linkage group does not contain a methylene "spacer" between the iodoacetamide reactive group and the fluorophore. This difference might account for its inability to be significantly quenched by tyrosine, and the possibility remains that some other BODIPY fluorophores may still show tyrosine-induced quenching, as has been reported in studies using free Tyr amino acid and BODIPY-FL.[44]

The observation that Tyr does not significantly quench BODIPY 507/545, whereas Trp does, suggests several possible uses. For example, when studying a protein of unknown structure or conformation, one could rapidly determine if some observed bimane quenching in an experiment is due to Trp or Tyr by simply relabeling the same protein with BODIPY 507/545. A lack of BODIPY 507/545 quenching would indicate the cause of the initial bimane quenching was a Tyr residue. Similarly, one could exploit the different quenching profiles obtained using Trp and Tyr to glean orientation information about how two interacting proteins dock with each other.

Both TrIQ and TyrIQ Can Detect a Hinge Bending Movement in T4L That Occurs with Substrate Binding. Crystal structures show binding of the substrate to T4L involves a large domain movement between two lobes that results in the exposure of the active site. We attempted to measure this movement by placing a quencher (Trp or Tyr) on one side of the active site cleft (residue 4) and a fluorescent probe on the other side (residue 60). Crystal structures show the Cα−Cα distances between these two sites are shorter (∼10.5 Å) in the empty state[45] and then become longer (∼14.5 Å) upon binding of the substrate.[33] The latter distances were determined using a T4L active site mutant T26E, which covalently binds and traps the substrate peptidoglycan.[33] This active site mutant has been used in numerous previous studies focused on defining this hinge bending;[34,39] thus, here we tested if this hinge bending could be detected using TrIQ or TyrIQ, which would result in a decreased level of quenching upon substrate binding.

Indeed, the TrIQ and TyrIQ data reflect the movements seen in the crystal structures. As seen in Figure 6, the Trp-containing sample shows significant quenching in the absence of substrate, but almost no quenching for the substrate-bound T26E mutant. In contrast, Tyr showed a very small amount of quenching for the substrate-free T4L and no quenching upon binding of the substrate to the T26E mutant.

These changes are exactly as one would expect on the basis of the distance-dependent constraints reported in the Results. As shown in Figures 3 and 5, the maximal reach is ∼15 Å for Trp, but only ∼10 Å for Tyr. Thus, significant Trp quenching and minimal Tyr quenching are expected for T4L in the apo, freely hinge-bending, state, as is observed (Figure 6). In contrast, no significant quenching should be expected for either Trp or Tyr in the substrate-bound state in the T26E mutant, as the two sites move 14.5 Å apart, outside of the maximal reach of either quenching residue.

Together, these observations show how including Tyr quenching increases the resolution of an internal quenching study, by allowing the separation of "very close" interaction distances (less than ∼10 Å) and those that are between ∼10 and ∼15 Å.

Arrhenius Analysis of the TrIQ and TyrIQ Data Suggests a Low Energy Barrier for Hinge Bending

Motion in T4L. We also assessed the energetics of the hinge bending movement, described above, by conducting studies at different temperatures and subjecting the results to Arrhenius analysis. Specifically, we calculated a dynamic quenching rate, K_q, at each temperature from the amplitude-weighted average lifetime, $\langle\tau\rangle$, as described previously in Materials and Methods, and used these values for Arrhenius analysis.[26,46] The similar low E_a values resulting from this analysis of both the TrIQ and TyrIQ data (~1.5−2.5 kcal/mol) are consistent with the idea that hinge bending movement between empty and substrate-bound T4L conformations occurs in the protein[39,40] and is not impeded by a high activation energy barrier. The E_a values obtained from TrIQ and TyrIQ differ by ~1 kcal, and it is not yet clear if the difference is truly significant, as the different physical properties of Trp and Tyr could cause a subtle difference in this dynamic movement in T4L. Moreover, the amount of quenching is low in the Tyr samples, and thus, the data could potentially contain significant error due to the weak signal and increased level of noise.

In summary, in this work we expanded the tool set for characterizing and quantifying dynamic structural movements in proteins by establishing and calibrating how Tyr can be used in internal quenching SDFL studies. We find that TrIQ and TyrIQ of bimane can be measured across a range of pHs and temperatures, and we show how the use of these two approaches together increases the resolution of structural and dynamics information that can be obtained, thus significantly expanding the scope of this SDFL approach.

Some caveats with regard to TrIQ and TyrIQ need be mentioned. First, in contrast to FRET, neither method has a straightforward and experimentally verified theory for mathematically calculating precise distances between the quencher and fluorophore. However, it is possible to identify and quantify quencher−probe pairs that are in the proximity of each other (dynamic quenching) and those in contact at the moment of light excitation (static quenching), although we are using these terms in an operational sense. It can also be difficult to separate "true" static quenching from "pseudo" static quenching, the latter of which occurs when ultrafast quenching events (due to excited-state collisions between proximal quencher−probe pairs immediately after light excitation) introduce ultrashort lifetime components into the data. Thus, in these calculations, it is critical to take into account the time resolution of the instrument and scattering propensity of the sample when calculating the fluorescence lifetimes and differentiating between light scattering and ultrafast quenching events. Second, for the bimane probe used here, both TrIQ and TyrIQ work over only a limited distance (<15 Å), although this limitation can also be considered a strength and used to increase the precision of a given measurement. Third, the use of Cα−Cα distance as a calibration metric is nonideal because it does not account for parameters like probe−quencher orientation. In the future, a key step to advancing the TrIQ and TyrIQ methods will be to include molecular dynamics simulations in the analysis of the data to model the quencher−probe interactions, as Ladhokin and colleagues have done using two Trp residues to approximate the Trp−bimane pair.[47]

Importantly, TyrIQ introduces new advantages to this internal quenching approach. For one thing, TyrIQ works over a range smaller than that of TrIQ and thus can be used to provide higher distance resolution. Furthermore, the fact that Tyr (the quencher) differs from the control (Phe) by only an -OH group means that TyrIQ studies will be optimal for use to minimize proteins sensitive to changes in steric volume. Previously, bimane TrIQ has been used to asses movements within GPCRs,[15,26,47−49] and we have recently begun using this approach to map the interactions between the GPCR opsin and visual arrestin.[22] Future efforts will explore the use of TyrIQ in these efforts, as well.

■ ASSOCIATED CONTENT

Supporting Information

Includes a discussion of the results obtained fitting the unquenched and quenched fluorescence decays using a lifetime distribution model (Lorentzian), tables of data (including calculated lifetimes for each sample resulting from the exponential fits and distribution fits), and quenching ratios for T4L T26E mutants in various ligand-bound states. Quantum yield analysis for T4L N116X/N132B samples, and figures of these samples demonstrating how the maximal absorbance of the bimane peak shifts due to static complex formation between quencher and fluorophore. Examples of exponential fitting of bimane fluorescent decay data, intensity quenching ratio bar graphs for BODIPY 507/545 quenching, intensity and lifetime quenching ratios for the varying pH and temperatures tested for bimane quenching, and an SDS-PAGE gel depicting the active site mutant T4L with and without peptidoglycan. This material is available free of charge via the Internet at http://pubs.acs.org.

■ AUTHOR INFORMATION

Corresponding Author

*E-mail: farrensd@ohsu.edu. Phone: (503) 494-0583. Fax: (503) 494-8393.

Funding

This work was supported by National Institutes of Health Grants R01 EY015436 and S10RR025684 (to D.L.F.) and Training Grant 5T32GM071338 (A.M.J.B.). We thanks the ARCS foundation of Portland and OHSU Tartar Trust for their generous support of A.M.J.B.

Notes

The authors declare no competing financial interest.

■ ACKNOWLEDGMENTS

We thank Dr. Steve Mansoor, Dr. Jon Fay, and Mr. Christopher T. Schafer for their critical reading of the manuscript and Owen Chapman.

■ ABBREVIATIONS

BODIPY 507/545, *N*-(4,4-difluoro-1,3,5,7-tetramethyl-4-bora-3a,4a-diaza-*s*-indacen-2-yl)iodoacetamide; EDTA, *N*,*N*′-1,2-ethanediylbis[*N*-(carboxymethyl)glycine] disodium salt; FRET, Forster resonance energy transfer; IPTG, isopropyl β-thiogalactoside; IRF, instrument response function; MOPS, 3-(*N*-morpholino)propanesulfonic acid; PDB, Protein Data Bank; SDFL, site-directed fluorescent labeling; SDS−PAGE, sodium dodecyl sulfate−polyacrylamide gel electrophoresis; T4L, T4 lysozyme; Tris, 2-amino-2-(hydroxylmethyl)-1,3-propanediol; TrIQ, tryptophan-induced quenching; TyrIQ, tyrosine-induced quenching; $\langle\tau\rangle$, amplitude-weighted average fluorescence lifetime; F_O/F, fluorescence intensity quenching ratio; τ_O/τ, fluorescence lifetime quenching ratio.

REFERENCES

(1) Alexiev, U., and Farrens, D. L. (2014) Fluorescence spectroscopy of rhodopsins: Insights and approaches. *Biochim. Biophys. Acta 1837*, 694−709.

(2) Caputo, G. A., and London, E. (2013) Analyzing transmembrane protein and hydrophobic helix topography by dual fluorescence quenching. *Methods Mol. Biol. 974*, 279−295.

(3) Daggett, K. A., and Sakmar, T. P. (2011) Site-specific in vitro and in vivo incorporation of molecular probes to study G-protein-coupled receptors. *Curr. Opin. Chem. Biol. 15*, 392−398.

(4) Dekel, N., Priest, M. F., Parnas, H., Parnas, I., and Bezanilla, F. (2012) Depolarization induces a conformational change in the binding site region of the M2 muscarinic receptor. *Proc. Natl. Acad. Sci. U.S.A. 109*, 285−290.

(5) Gasymov, O. K., Abduragimov, A. R., and Glasgow, B. J. (2012) Tryptophan rotamer distribution revealed for the α-helix in tear lipocalin by site-directed tryptophan fluorescence. *J. Phys. Chem. B 116*, 13381−13388.

(6) Ho, D., Lugo, M. R., and Merrill, A. R. (2013) Harmonic analysis of the fluorescence response of bimane adducts of colicin E1 at helices 6, 7, and 10. *J. Biol. Chem. 288*, 5136−5148.

(7) Kim, Y. J., Hofmann, K. P., Ernst, O. P., Scheerer, P., Choe, H. W., and Sommer, M. E. (2013) Crystal structure of pre-activated arrestin p44. *Nature 497*, 142−146.

(8) Raghuraman, H., Islam, S. M., Mukherjee, S., Roux, B., and Perozo, E. (2014) Dynamics transitions at the outer vestibule of the KcsA potassium channel during gating. *Proc. Natl. Acad. Sci. U.S.A. 111*, 1831−1836.

(9) Rasmussen, S. G., Choi, H. J., Fung, J. J., Pardon, E., Casarosa, P., Chae, P. S., Devree, B. T., Rosenbaum, D. M., Thian, F. S., Kobilka, T. S., Schnapp, A., Konetzki, I., Sunahara, R. K., Gellman, S. H., Pautsch, A., Steyaert, J., Weis, W. I., and Kobilka, B. K. (2011) Structure of a nanobody-stabilized active state of the β_2 adrenoceptor. *Nature 469*, 175−180.

(10) Sasaki, J., Phillips, B. J., Chen, X., Van Eps, N., Tsai, A. L., Hubbell, W. L., and Spudich, J. L. (2007) Different dark conformations function in color-sensitive photosignaling by the sensory rhodopsin I-HtrI complex. *Biophys. J. 92*, 4045−4053.

(11) Taraska, J. W. (2012) Mapping membrane protein structure with fluorescence. *Curr. Opin. Struct. Biol. 22*, 507−513.

(12) Venezia, C. F., Meany, B. J., Braz, V. A., and Barkley, M. D. (2009) Kinetics of association and dissociation of HIV-1 reverse transcriptase subunits. *Biochemistry 48*, 9084−9093.

(13) Yao, X., Parnot, C., Deupi, X., Ratnala, V. R., Swaminath, G., Farrens, D., and Kobilka, B. (2006) Coupling ligand structure to specific conformational switches in the β2-adrenoceptor. *Nat. Chem. Biol. 2*, 417−422.

(14) Doose, S., Neuweiler, H., and Sauer, M. (2005) A close look at fluorescence quenching of organic dyes by tryptophan. *ChemPhysChem 6*, 2277−2285.

(15) Fay, J. F., and Farrens, D. L. (2012) A key agonist-induced conformational change in the cannabinoid receptor CB1 is blocked by the allosteric ligand Org 27569. *J. Biol. Chem. 287*, 33873−33882.

(16) Islas, L. D., and Zagotta, W. N. (2006) Short-range molecular rearrangements in ion channels detected by tryptophan quenching of bimane fluorescence. *J. Gen. Physiol. 128*, 337−346.

(17) Janz, J. M., and Farrens, D. L. (2004) Rhodopsin activation exposes a key hydrophobic binding site for the transducin α-subunit C terminus. *J. Biol. Chem. 279*, 29767−29773.

(18) Mansoor, S. E., Dewitt, M. A., and Farrens, D. L. (2010) Distance mapping in proteins using fluorescence spectroscopy: The tryptophan-induced quenching (TrIQ) method. *Biochemistry 49*, 9722−9731.

(19) Mansoor, S. E., and Farrens, D. L. (2004) High-throughput protein structural analysis using site-directed fluorescence labeling and the bimane derivative (2-pyridyl)dithiobimane. *Biochemistry 43*, 9426−9438.

(20) Mansoor, S. E., McHaourab, H. S., and Farrens, D. L. (2002) Mapping proximity within proteins using fluorescence spectroscopy. A study of T4 lysozyme showing that tryptophan residues quench bimane fluorescence. *Biochemistry 41*, 2475−2484.

(21) Semenova, N. P., Abarca-Heidemann, K., Loranc, E., and Rothberg, B. S. (2009) Bimane fluorescence scanning suggests secondary structure near the S3-S4 linker of BK channels. *J. Biol. Chem. 284*, 10684−10693.

(22) Sinha, A., Brunette, A. M., Fay, J. F., Schafer, C. T., and Farrens, D. L. (2014) Rhodopsin TM6 can Interact with two Separate and Distinct Sites on Arrestin: Evidence for Structural Plasticity and Multiple Docking Modes in Arrestin-Rhodopsin Binding. *Biochemistry 53*, 3294−3307.

(23) Sommer, M. E., Farrens, D. L., McDowell, J. H., Weber, L. A., and Smith, W. C. (2007) Dynamics of arrestin-rhodopsin interactions: Loop movement is involved in arrestin activation and receptor binding. *J. Biol. Chem. 282*, 25560−25568.

(24) Tapley, T. L., Cupp-Vickery, J. R., and Vickery, L. E. (2005) Sequence-dependent peptide binding orientation by the molecular chaperone DnaK. *Biochemistry 44*, 12307−12315.

(25) Tapley, T. L., and Vickery, L. E. (2004) Preferential substrate binding orientation by the molecular chaperone HscA. *J. Biol. Chem. 279*, 28435−28442.

(26) Tsukamoto, H., and Farrens, D. L. (2013) A constitutively activating mutation alters the dynamics and energetics of a key conformational change in a ligand-free G protein-coupled receptor. *J. Biol. Chem. 288*, 28207−28216.

(27) Doose, S., Neuweiler, H., and Sauer, M. (2009) Fluorescence quenching by photoinduced electron transfer: A reporter for conformational dynamics of macromolecules. *ChemPhysChem 10*, 1389−1398.

(28) Sato, E., Sakashita, M., Kanaoka, Y., and Kosower, E. M. (1988) Organic fluorescent reagents: XIV. Novel Fluorogenic Substrates for Microdetermination of Chymotrypsin and Aminopeptidase: Bimane Fluorescence Appears after Hydrolysis. *Bioorg. Chem. 16*, 298−306.

(29) Hayashibara, M., and London, E. (2005) Topography of diphtheria toxin A chain inserted into lipid vesicles. *Biochemistry 44*, 2183−2196.

(30) Sathish, H. A., Stein, R. A., Yang, G., and McHaourab, H. S. (2003) Mechanism of chaperone function in small heat-shock proteins. Fluorescence studies of the conformations of T4 lysozyme bound to αB-crystallin. *J. Biol. Chem. 278*, 44214−44221.

(31) Taraska, J. W., Puljung, M. C., and Zagotta, W. N. (2009) Short-distance probes for protein backbone structure based on energy transfer between bimane and transition metal ions. *Proc. Natl. Acad. Sci. U.S.A. 106*, 16227−16232.

(32) Vincelli, A. J., Pottinger, D. S., Zhong, F., Hanske, J., Rolland, S. G., Conradt, B., and Pletneva, E. V. (2013) Recombinant expression, biophysical characterization, and cardiolipin-induced changes of two *Caenorhabditis elegans* cytochrome c proteins. *Biochemistry 52*, 653−666.

(33) Kuroki, R., Weaver, L. H., and Matthews, B. W. (1993) A covalent enzyme-substrate intermediate with saccharide distortion in a mutant T4 lysozyme. *Science 262*, 2030−2033.

(34) Yirdaw, R. B., and McHaourab, H. S. (2012) Direct observation of T4 lysozyme hinge-bending motion by fluorescence correlation spectroscopy. *Biophys. J. 103*, 1525−1536.

(35) Abdulaev, N. G., Zhang, C., Dinh, A., Ngo, T., Bryan, P. N., Brabazon, D. M., Marino, J. P., and Ridge, K. D. (2005) Bacterial expression and one-step purification of an isotope-labeled heterotrimeric G-protein α-subunit. *J. Biomol. NMR 32*, 31−40.

(36) Lakowicz, J. R. (2006) *Principles of fluorescence spectroscopy*, 3rd ed., Springer, New York.

(37) Mansoor, S. E., McHaourab, H. S., and Farrens, D. L. (1999) Determination of protein secondary structure and solvent accessibility using site-directed fluorescence labeling. Studies of T4 lysozyme using the fluorescent probe monobromobimane. *Biochemistry 38*, 16383−16393.

(38) Closs, G. L., and Miller, J. R. (1988) Intramolecular long-distance electron transfer in organic molecules. *Science 240*, 440−447.

(39) McHaourab, H. S., Oh, K. J., Fang, C. J., and Hubbell, W. L. (1997) Conformation of T4 lysozyme in solution. Hinge-bending motion and the substrate-induced conformational transition studied by site-directed spin labeling. *Biochemistry 36*, 307–316.
(40) Zhang, X. J., Wozniak, J. A., and Matthews, B. W. (1995) Protein flexibility and adaptability seen in 25 crystal forms of T4 lysozyme. *J. Mol. Biol. 250*, 527–552.
(41) Spencer, R. D. (1970) Fluorescence lifetimes: Theory, instrumentation, and application or nanosecond fluorometry. Ph.D. Dissertation, Department of Chemistry, University of Illinois at Urbana-Champaign, Urbana, IL.
(42) Harriman, A. (1987) Further Comments on the Redox Potentials of Tryptophan and Tyrosine. *J. Phys. Chem. 91*, 3.
(43) Torimura, M., Kurata, S., Yamada, K., Yokomaku, T., Kamagata, Y., Kanagawa, T., and Kurane, R. (2001) Fluorescence-quenching phenomenon by photoinduced electron transfer between a fluorescent dye and a nucleotide base. *Anal. Sci. 17*, 155–160.
(44) Marme, N., Knemeyer, J. P., Sauer, M., and Wolfrum, J. (2003) Inter- and intramolecular fluorescence quenching of organic dyes by tryptophan. *Bioconjugate Chem. 14*, 1133–1139.
(45) Weaver, L. H., and Matthews, B. W. (1987) Structure of bacteriophage T4 lysozyme refined at 1.7 Å resolution. *J. Mol. Biol. 193*, 189–199.
(46) Shi, X., Duft, D., and Parks, J. H. (2008) Fluorescence quenching induced by conformational fluctuations in unsolvated polypeptides. *J. Phys. Chem. B 112*, 12801–12815.
(47) Ghanouni, P., Gryczynski, Z., Steenhuis, J. J., Lee, T. W., Farrens, D. L., Lakowicz, J. R., and Kobilka, B. K. (2001) Functionally different agonists induce distinct conformations in the G protein coupling domain of the β2 adrenergic receptor. *J. Biol. Chem. 276*, 24433–24436.
(48) Ghanouni, P., Steenhuis, J. J., Farrens, D. L., and Kobilka, B. K. (2001) Agonist-induced conformational changes in the G-protein-coupling domain of the β2 adrenergic receptor. *Proc. Natl. Acad. Sci. U.S.A. 98*, 5997–6002.
(49) Tsukamoto, H., Farrens, D. L., Koyanagi, M., and Terakita, A. (2009) The magnitude of the light-induced conformational change in different rhodopsins correlates with their ability to activate G proteins. *J. Biol. Chem. 284*, 20676–20683.